JP1.9 MULTI-CHANNEL ANALYSES OF WARM CLOUD DROPLET SIZE FOR GLOBAL SCALE

Takashi Y. Nakajima *
Earth Observation Research Center, NASDA , Tokyo, Japan
Teruyuki Nakajima
Center for Climate System Research, University of Tokyo, Tokyo, Japan

1. INTRODUCTION

Cloud microphysical properties, such as optical thickness and effective radius, were retrieved by using a nonabsorbing channel (e.g. 0.64 μm of AVHRR), a water-absorbing channel (e.g. 3.75μm), and a thermal channel (e.g. 11 μm). Nakajima and Nakajima (1995) demonstrated that the retrievals were accurate enough to distinguish artificial and natural transformations of cloud properties. Utilization of the 3.75-μm channel was thus a realistic choice for the cloud retrievals from reflected solar radiance. One reason for using the 3.75-μm channel as the water-absorbing channel was that most previous satellite-borne sensors, such as AVHRR, were equipped only with this channel in the near-infrared wavelength domain. However, most modern sensors are equipped with more channels at near-infrared wavelengths. For example, VIRS aboard the TRMM satellite has both 1.6- and 3.7-μm channels; MODIS aboard the Terra satellite and GLI aboard the ADEOS-II satellite have 1.6-, 2.2- and 3.7-μm channels (or nearby). The imaginary indices of refraction of liquid water at these wavelengths are, ~ 10^{-5} (1.6-μm), ~ 10^{-4} (2.2-μm), and ~ 10^{-3} (3.7-μm), and they are still larger than 0.63-μm channel's ~ 10^{-9}, so that 1.6-μm and 2.2-μm channels, in addition to the 3.7-μm channel are sensitive to cloud droplet sizes. Therefore, it is natural to have interest in retrieving cloud effective radius and investigating the differences among them, if any, by using these extended channels. Curran and Wu (1982) retrieved the cloud effective radius by using 1.6- and 2.2-μm channels from the Skylab radiometer. Then results indicated that the effective radius retrieved at 2.2 μm differed from that retrieved at 1.6 μm. However, their retrievals were performed only at eight points in a scene taken over New Mexico in North America. In this section, we tried to retrieve the global distribution of effective radii by using the 2.1-μm channel of MODIS aboard the Terra as well as 3.7-μm channels and compare them to get the difference of effective radii values. This work is the first to estimate this difference. It is noteworthy that using 1.6- and/or 2.2-μm (or nearby) channels has an advantage over using the 3.7-μm channel because the former channels don't include undesirable thermal components included in 3.7-μm channels.

*Corresponding author address: Takashi Y. Nakajima, Earth Observation Research Center,
National Space Development Agency of Japan
1-8-10, Harumi, Chuo-ku, Tokyo 104-6023, Japan*

2. EXTENSION FROM NAKAJIMA AND NAKAJIMA 1995

Cloud retrievals using the solar reflection method we used enhanced Eq. (4) from Nakajima and Nakajima (1995) so that radiances, transmissivities, plane albedo, and spherical albedo were independent from model atmospheres, especially water vapor effects, and so that thermal emission from atmospheric layers other than cloud layers can be subtracted. Eq. (1) is an enhanced equation.

$$
\begin{aligned}
L(w_u,w_c,\tau,r_e;\mu,\mu_0,\phi) = {} & L_{obs}(w_u,w_c,\tau,r_e;\mu,\mu_0,\phi) \\
& -t(w_u,\tau_u,\mu)\left[1-t(w_c,\tau_c,r_e;\mu)-r(w_c,\tau_c,r_e;\mu)\right]B(T_c) \\
& -t(w_u,w_c,\tau,r_e;\mu)\frac{1-A_g}{1-\bar{r}(w_u,w_c,\tau,r_e)A_g}B(T_g) \\
& -t(w_u,w_c,\tau,r_e;\mu)\frac{A_g}{1-\bar{r}(w_u,w_c,\tau,r_e)A_g}t(w_u,w_c,\tau,r_e;\mu_0)\frac{\mu_0F_0}{\pi} \\
& -L_{tml}(w_u,T_c) \\
& -t(w_u,\tau_u,\mu)t(w_c,\tau_c,r_e;\mu)L_{tml}(w_d,T_g)
\end{aligned} \quad .\ (1)
$$

In Eq. (1), w_u, w_c, and w_d are the equivalent water vapor amounts defined as

$$w_{u,c,d} = \int_{z_1}^{z_2} w(z)\left(\frac{P(z)}{P_g}\right)^{0.5}\left(\frac{T_g}{T(z)}\right)^{0.9} dz,$$

where, z_1 and z_2 are ground level and cloud bottom, cloud bottom and cloud top, cloud top and top of atmosphere, for w_u, w_c; w_d. $w(z)$, $P(z)$ and $T(z)$ are the vertical profiles of water vapor, air pressure, and air temperature as a function of altitude z; P_g and T_g are surface pressure and temperature. These objective analysis quantities were obtained from global objective analysis data (GANAL) of the Japan Meteorological Agency (JMA). Kawamoto et al. (2001) showed that undesirable thermal emission components from atmospheric layers above the cloud (fifth term of Eq. (1)) and below the cloud (sixth term of Eq. (1)) that were not subtracted in Eq. (4) from Nakajima and Nakajima (1995) can be fitted by using parameters of $w_uB(T_c)$ and $w_dB(T_g)$, respectively. Although, Kawamoto et al. (2001) used the same grid system as used in this method, we modified it in this thesis so that radiances, transmissivities, plane albedo, and spherical albedo in Eq. (1) are expressed by the equivalent waver vapor ($w_{u,,}$,$w_{c,,}$ = 50, 5000, 10000, 20000, 30000, 40000, 50000 g/m^2 of the lookup table grid) as a replacement for Z and D grids. Moreover, we changed the iteration scheme from the two-dimensional bisection method used in Nakajima and Nakajima 1995 and Kawamoto et al. 2001 to the three-dimensional Newton-Raphson method. This scheme simultaneously retrieves τ_c, r_e, and T_c. These modifications advance the decoupling process of the undesirable radiation components and increase iteration efficiency about five times. Figure 1 illustrates the latest flow of analysis.

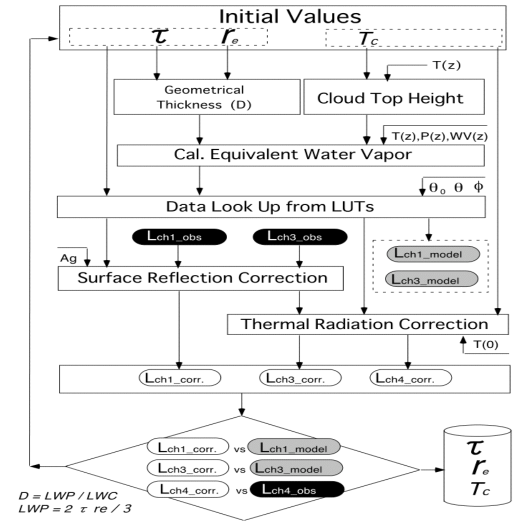

FIG. 1 Flow of analysis.

3. RESULTS

Figures 2, 3, and 4 illustrate the global distribution of the retrieved effective radii of low-level clouds with T_c above 273 K, using 0.87μm-2.1μm-10.8μm channels (r_e_2.1) and 0.87μm-3.7μm-10.8μm channels (r_e_3.7) of MODIS aboard the Terra satellite, and ratio of r_e_2.1 to r_e_3.7, respectively. The results are a one-month average of September 13 to October 12, 2000. The global-segmented datasets of radiances for MODIS were used as shown. A similar segment was defined by Kawamoto et al. (2001). Briefly, one segment box has

TABLE 1 Comparisons of obtained optical thickness and effective radius over ocean and land area in autumn season.

References	Water-absorbing channel	Optical Thickness (τ_c)		Effective Radius (r_e μm)	
		Ocean	Land	Ocean	Land
Han et al. 1994 (*1)	3.7 μm	6.9	8.5	12.2	8.0
Kawamoto et al. 2001 (*2)	3.7 μm	4.8	5.6	12.7	9.2
MODIS (This work) (*3)	3.7 μm	7.9	11.2	13.7	10.0
MODIS (This work) (*3)	2.1 μm	8.6	12.9	14.3	12.3

(*1) One-month average in October 1987 and 1988 obtained from AVHRR.
(*2) One-month average in October 1987 obtained from AVHRR.
(*3) One-month average (September 13 - October 12 in 2000) obtained from MODIS

0.5° x 0.5° spatial resolution, and there are 720 x 360 boxes in the analysis region of the –90° to +90° latitude domain. Twenty-five pixels are stored in one segment box (a hundred pixels are stored in one segment box in Kawamoto et al. 2001).

In Figs. 2 and 3, the effective radii over land areas are smaller than over ocean areas. The averaged differences between land and ocean areas are 2.0 μm for r_e_2.1 and 3.7 μm in r_e_3.7. Moreover, smaller effective radii were observed in aerosol-rich regions such as off the west coast of north and South Africa, and the Arabian Peninsula, as reported by Higurashi and Nakajima (1999) as well as off eastern Asia. These features are qualitatively consistent with the results of Han et al. (1994) and Kawamoto et al. (2001). Table 1 summarizes the obtained optical thicknesses and effective radii from many sources. MODIS observation always overestimated values compared with other observations. These differences will be due to calibration of radiometric signals, the cloud masking method used in each observation, and/or different observation periods. However, MODIS results may be more accurate than other observations because MODIS is a newer sensor, designed and developed with more advanced techniques than available in the AVHRR *era*. The ratio of r_e_2.1 to r_e_3.7 (Fig. 3) has unique features. The ratio reached 2 over low-latitude land areas, but was almost 1 over ocean areas. We considered three reasons for this phenomenon, the effect of sub-pixel size clouds (land contamination), the difference instantaneous field of view (IFOV) of MODIS 2.1- (500m) and 3.7-μm (1 km) channels, and calibration problems. A vertical profile of the cloud droplet size can also influence the results. If the cloud droplets near the cloud top are smaller than those in the middle or bottom layers due to the evaporation stage with entrainment, r_e_2.1 will be larger than r_e_3.7 because the 2.1-μm channel data has information of clouds deeper than acquired by 3.7-μm channel due to the relatively small imaginary index of refraction. The results in this section indicate that we must further investigate obtained microphysical parameters. Hence, further comparisons between satellite-derived results and *in situ* results acquired from aircraft are needed.

Acknowledgement

MODIS aboard on Terra data were supplied from NASA/GSFC/DAAC. The research was partly supported by NASDA GLI science project and CREST Japan Science and Technology Corporation.

References

Curran, R. J., and M. L. C. Wu, 1982: Skylab near-infrared observations of clouds indicating supercooled liquid water droplets. *J. Atmos. Sci.*, **39**, 635-647

Han, Q., W. B. Rossow, and A. A. Lacis, 1994: Near-global survey of effective droplet radii in liquid water clouds using ISCCP data. *J. Climate*, **7**, 465-497.

Higurashi, A. and T. Nakajima, 1999: Development of a two channel aerosol retrieval algorithm on global scale using NOAA/AVHRR, *J. Atmos. Sci.,* **56**, 924-941.

Kawamoto. K, T. Nakajima, and T. Y. Nakajima, 2001: A global determination of cloud microphysics with AVHRR remote sensing. *J. Climate*, **14**, 2054-2068.

Nakajima T. Y. and T. Nakajima, 1995: Wide-area determination of cloud microphysical properties from NOAA AVHRR measurement for FIRE and ASTEX regions. *J. Atmos. Sci.*, **52**, 4043-4059.

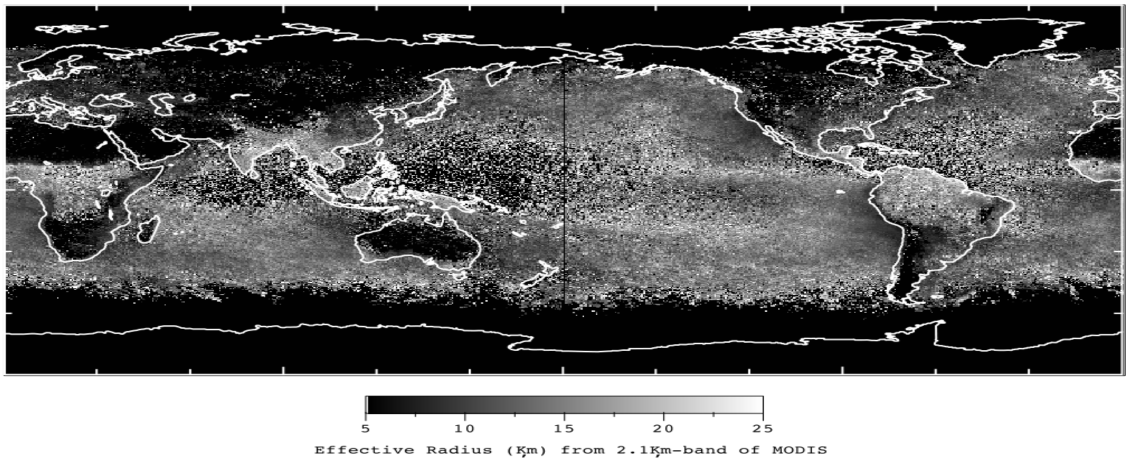

FIG. 2 One-month average of the effective radius of clouds with cloud top temperature warmer than 273K obtained by 0.87μm-2.1μm-10.8μm of MODIS aboard the Terra satellite.

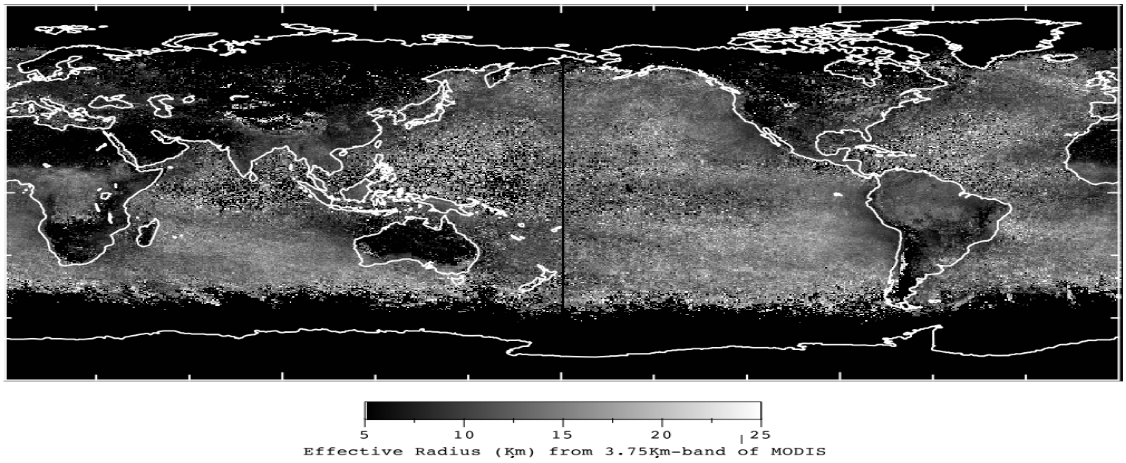

FIG. 3 As Fig.2 except for 0.87μm-3.7μm-10.8μm uses.

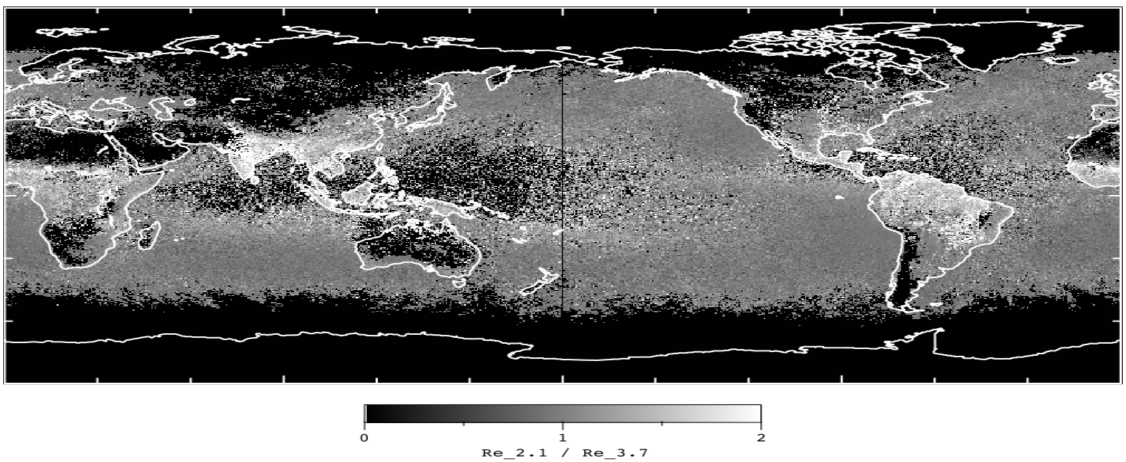

FIG. 4 Ratio of Fig.2 to Fig. 3